Soft Matter

View Online
Dynamic Article Links

Cite this: *Soft Matter*, 2011, **7**, 8182

www.rsc.org/softmatter

PAPER

Raft registration across bilayers in a molecularly detailed model

Diego A. Pantano,*[a] Preston B. Moore,[b] Michael L. Klein[c] and Dennis E. Discher[a]

Received 22nd March 2011, Accepted 25th May 2011
DOI: 10.1039/c1sm05490b

Coupling between the inner and outer leaflets of a bilayer plays an important role in biomembrane function, particularly in inducing and registering rafts across leaflets for various cellular signals. However, mechanisms of raft registration remain elusive and several alternatives have been proposed, ranging from electrostatic coupling to chain interdigitation, cholesterol flip-flop and composition-curvature coupling. A general mechanism has been suggested by recent experiments with mixtures of polymer amphiphiles that exhibit domain registration upon ligand-induced segregation. Here, using coarse grained molecular dynamics (CGMD) simulations that are rooted in atomistics, we show that raft registration arises spontaneously in bilayers with a calcium- or ligand-crosslinked ordered phase segregating from a liquid disordered phase. When rafts are not registered, a thickness mismatch between phases induces a "bump" in the apposing liquid phase leaflet, and it appears that the associated localized curvature change guides rafts together and stabilizes the registered state. The absence of explicit charge in the model and the fact that domain size modulates the strength of transmembrane coupling demonstrate that collective interactions are sufficient for raft registration.

1. Introduction

Lateral heterogeneity of lipids within biological membranes is increasingly accepted with so-called membrane rafts[1,2] helping to compartmentalize a number of key cellular processes. Lipid raft domains reportedly vary in size from 10 nm to 200 nm and are rich in sterol- and sphingolipids, suggesting highly specialized interactions,[3] but by definition raft interactions are collective and cooperative. The two bilayer leaflets of cell membranes are also asymmetric in composition[4] and tend to segregate: lipid mixtures that are typically found in the outer (extracellular) leaflet of the plasma membrane phase-separate when reconstituted as model membranes but this does not typically occur with lipid mixtures that represent the inner, cytoplasmic, leaflet.[5] Despite leaflet differences, domains in one leaflet seem to induce segregation in the opposite leaflet and numerous mechanisms have been proposed: (*i*) coupling by transmembrane proteins that show an affinity for rafts,[6] (*ii*) interfacial energy minimization,[7] (*iii*) electrostatic coupling,[8] (*iv*) lipid[9] and cholesterol[10–12] flip- flop, (*v*) dynamic chain interdigitation,[8,13] (*vi*) van der Waals interactions and (*vii*) composition-curvature coupling.[14] Interdigitation had previously been discarded[15,16] but is lately reconsidered.[8]

Since its origins[17] the raft theory was used to explain key aspects of cell physiology and more recently stem cell differentiation[18–20] as well as the pathogenesis of several diseases.[21] Raft domains are nonetheless difficult to characterize in intact cells. Raft-mimicking model membranes such as giant unilamellar vesicles (GUVs), and planar solid-supported phospholipid films yield domains that are much easier to detect due to their large size.[22–29] Plasma membranes isolated from cells can also exhibit visible domains.[6,30] Recently, the binding of a physiological signaling ligand such as calcium within a mixture of neutral and polyanionic amphiphiles has been shown to induce domains in diverse self-assemblies such as bilayer vesicles and micelles:[31] divalent cations crossbridge the polyanionic amphiphiles inducing demixing from the neutral amphiphiles and generating spots or rafts within bilayer vesicles as well as stripes within cylindrical micelles made with synthetic diblock copolymers. Similar results have been reported for the inner leaflet signaling lipid phosphatidylinositol (PIP_2),[32,33] although the use of synthetic polymers has the major advantage of generating morphologies that are highly stable[34–37] while still tunable with pH and salt concentration.[38] Imaging has made it clear that cation-induced gel domains in one leaflet of a bilayer register with domains of the same size in the other leaflet; thus only two intensities (I_{gel} and $I_{fluid} = 0$) are measurable on vesicles, whereas any mis-registration would have produced three intensities ($2I_{gel}$, $1I_{gel}$ and $I_{fluid} = 0$). This ligand-induced transbilayer coupling of rafts is simulated here.

Previous explanations of raft registration have postulated interleaflet coupling that is typically based on a composition-dependent interfacial energy.[8] Mean-field models[39] as well as

[a]*Chemical and Biomolecular Engineering, University of Pennsylvania, 220 South 33rd Street, Philadelphia, PA, 19104-6393, USA. E-mail: discher@seas.upenn.edu*
[b]*Department of Chemistry & Biochemistry, University of the Sciences in Philadelphia (USP), 600 South 43rd St., Philadelphia, PA, 19104-4496, USA*
[c]*Department of Chemistry, Temple University, 1901 N. 13th Street, Philadelphia, PA, 19122, USA*

molecular simulations around the registered equilibrium position[40] have led to estimates for the tension. The work presented here extends into the non-equilibrium regime of raft registration. In previous simulations[41] demixing resulted from differential interactions between lipid tails, but here we induce strong lateral segregation in homogeneous tail-groups by adding "ions" that crosslink head-groups. The resulting rafts exhibit a higher order compared with the surrounding liquid phase. Our approach involves a model of generic polymer mixtures but the conclusions seem applicable to any raft-mimicking bilayers, whether composed of natural lipid or a synthetic polymer amphiphile. Importantly, the non-ionic nature of the model minimizes the role of electrostatic coupling in registering such domains and reinforces the role for differential order and collective phenomena.

2. Model

The system models a binary mixture of (charged and neutral) surfactants in explicit water plus cross-linker particles which mimic calcium. A CG model for nonionic PEG (polyethylene glycol) based surfactants was developed by Shinoda *et al.*[42] using detailed atomistics of solvation, bond stretching and bending. We have recently shown[43] that minimal modifications to this model prove sufficient to reproduce experiments showing bilayer and micellar morphologies of charged polymers at different pH and cation concentrations[31,38] but without the inclusion of explicit charges in simulation. Here we used both models to understand mixtures of neutral (N-type) and "charged" (C-type) surfactants in water plus cross-linker "ion" type particles (L-type). N-type and C-type surfactants are very similar here with the only difference being the modified headgroup beads that mimic charged groups in strongly attracting the L-type particles which drive crosslinking. The strength of this interaction as well as the size of the L-type particles had been modulated to drive lateral segregation in the mixed surfactant system.[43] All CG bead sizes are comparable, with Lennard-Jones potential σ parameters (where the potential equals zero) ranging between 4 and 7 Å. The chains are flexible but short in order to minimize entanglements and allow for reasonable sampling of the dynamical processes. The absence of charges also resulted in faster computations since no long range forces are treated.

Both C-type and N-type polymers here have identical lengths of hydrophobic (aliphatic chain) and hydrophilic (polycarboxylic or PEG) parts. $C_{22}E_5$ ($C_{24}E_2$) surfactants are composed of 7(8) hydrophobic and 5(2) hydrophilic beads. The C-type surfactants have a fractional degree of ionization $\alpha = 0.5$–0.6 (*i.e.* 3 "charged" beads out of 5 for $C_{22}E_5$). For polycarboxylic acids this α corresponds to a pH $\sim$ 6.5.[43] In our simulations all "charged" surfactants are identical, *i.e.* they have the same α with ionized beads in the same position. Such correlated ionization seems reasonable because of the cooperative effects that increase the isoelectric point of polycarboxylic acids from the pH $\sim$ 4.5 that is typical of monomeric carboxylic acid. We tested polymer mixtures with different weights of hydrophilic fraction ($f \sim 0.21$ for $C_{24}E_2$ and $f \sim 0.46$ for $C_{22}E_5$) and systems with different C-type : N-type ratios (25 : 75 and 50 : 50) as studied in experiment.[31] There is one L-type particle for every two "charged" beads in the C-type headgroup. To eliminate possible artifacts from finite size effects on the registration process we tested bilayer domains ranging from 100 Å × 100 Å to 200 Å × 200 Å with no significant differences detected. All simulations were performed using the LAMMPS package[44] and visualized with VMD.[45] Isothermal-isobaric (NPT) and microcanonical (NVE) ensembles were employed in the simulations with $T = 298$ K and $P = 1$ atm. For the potential of mean force (PMF) calculation, the steered molecular dynamics method was employed as implemented in LAMMPS.[46,47]

Simulations were started from a completely random mixture of water, polymers (C and N types) and L particles. These runs helped establish the stability of the bilayer under the respective simulation conditions over μs time scales. The initial random configuration has the advantage of establishing the spontaneous, self-assembled nature of the bilayer but the disadvantage of obtaining systems where the number of C and N type molecules is not balanced on both sides of the bilayer. Once the bilayer was formed the composition of each leaflet remained close to a constant value although sporadic flip-flop transitions are observed within what will be identified later as a liquid disordered phase. To simplify analysis of the registration process we switched amphiphile identities as needed to start with a bilayer having an equal distribution of C and N type polymers in both leaflets.

3. Results and discussion

3.1 Domain formation and characterization

In every system studied here regardless of size, composition, or amphiphilic proportions, bilayer assembly was followed by formation of C-domains composed of C-type molecules and L-type particles. Several small aggregates per leaflet were observed initially, and these drifted and coalesced into one large domain per leaflet (Fig. 1). This of course minimizes any boundary energy. Detailed inspection of the snapshots reveals that the size of the aggregates is correlated to both condensation of the L-type particles within C-domains and the degree of stretching of the polymers within: the larger the domain, the more stretched, ordered, and close-packed the polymers and linker particles are. In the final segregated state, condensed L-type particles are in contact with up to 6 different C-type molecules as evidenced by the domain images in Fig. 1. The N-type polymers remain as a liquid phase that surrounds the domains. The complete demixing of C from N is consistent with the strong lateral segregation limit characterized in experiment, but there are many potential mechanisms for phase separation. Simulations here will later show that domain formation requires crosslinkers and is not based on length mismatches because (*i*) removal of the L-type crosslinkers leads to domain disassembly, and (*ii*) no assembly occurs with N-type molecules in which half of the molecules are stretched.

To quantify the molecular stretching inside and outside the domains, the average of the head-tail distance was determined as:

$$\langle r_{HT}(t)\rangle = \langle \|\mathbf{r}_{head}(t) - \mathbf{r}_{tail}(t)\|\rangle$$

where $\mathbf{r}_{head}$ and $\mathbf{r}_{tail}$ are the coordinates of a single polymer head and tail respectively. Molecular order was quantified by the

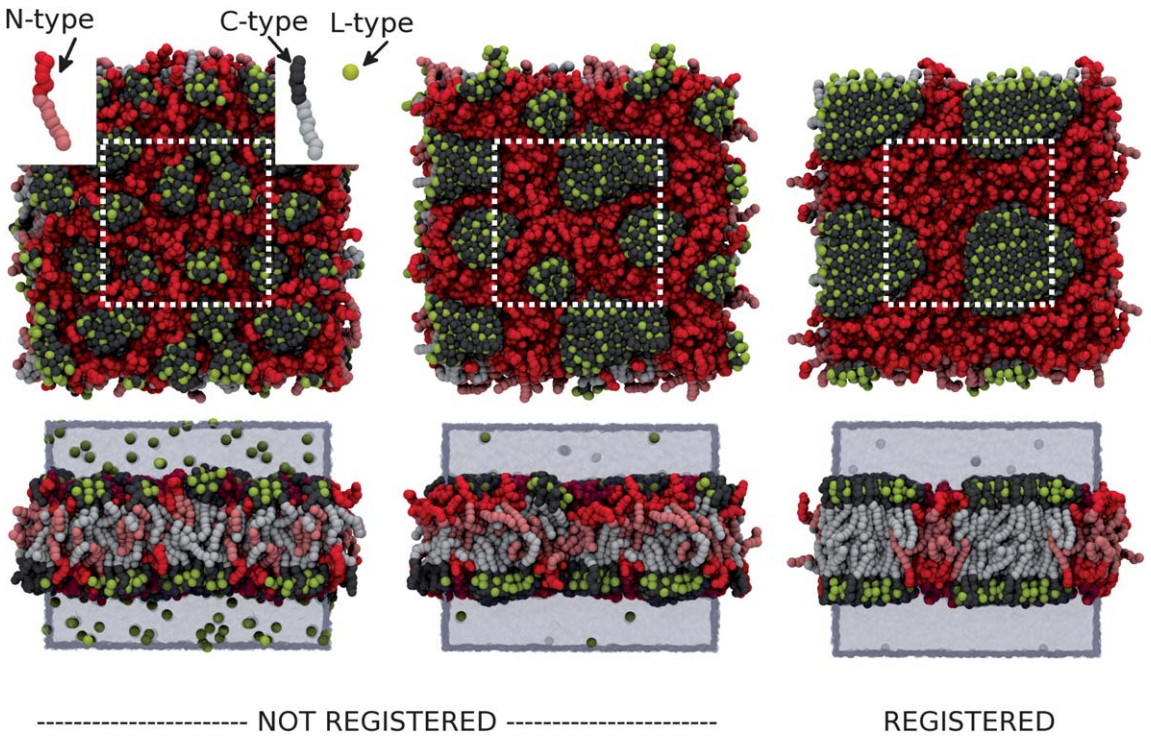

Fig. 1 Snapshots show the time evolution of domain coalescence and registration. Top: topview of the bilayer where water and non-bound L-type particles were removed. Bottom: lateral views of the same system. Upper inset shows the N-type (red and pink) and C-type (gray and white) polymers as well as the L-type particles (yellow). Water is represented by light blue. The white dashed lines delimit the periodic simulation box. From left to right: the small C-type particle domains coalesce to one per leaflet as the L-type particles condense into the "charged" headgroups. Only the final domains appear registered.

dynamical average of the second Legendre polynomial typical in the analysis of liquid crystalline materials:

$$\left\langle P_2(cos\ \theta;t)\right\rangle = \left\langle \frac{3\ cos^2\theta(t)-1}{2}\right\rangle$$

where θ is the angle between the polymer head-tail vector and the perpendicular to the bilayer. This quantifies the orientation of the polymers ranging from 0 (isotropic sample) to 1 (perfectly aligned sample). The time series for these observables are shown in Fig. 2 (A and B) for both types of polymers. The C-type polymers start out only slightly more stretched and ordered than N-type polymers, and by ~0.3 μs the C-type become more stretched and more ordered ($< P_2 > \sim 0.8$) whereas the N-type remain unchanged and exhibit an order halfway between nematic and isotropic. In addition to the C-type becoming more oriented with the bilayer normal, the smaller fluctuations show narrower distributions in both orientation and stretching—characteristic of a more crystalline or gel-like state. The above measure two aspects of order in this system, namely molecular stretching order, and rotational order, and there is at least one more order parameter here namely lateral order. All are increased with calcium-crossbridging of C-type chains.

The spotted domains observed experimentally in polymer vesicles[31] were circular in shape rather than faceted, and of course a circular domain implies a liquid or soft gel-like state. We were able to affect the aggregate shape through the molecular proportions of the polymer: small headgroups leave little space for the hydrophobic tails and strongly confined tails cannot do anything but stretch, thereby generating a crystalline-like domain. In contrast, larger headgroups allow more freedom for the tails and yield a gel-like state. To quantify circularity we use the domain isoperimetric quotient (Q) which relates the area of the domain to a circle of the same perimeter. It is defined first in terms of domain area A and perimeter L

$$Q = \frac{4\pi A}{L^2} \approx \pi^2 \frac{N_T}{N_p^2},$$

but with $2r$ as the average distance in the bilayer plane between nearest neighbor surfactants, the perimeter and area can be simplified to $L \approx 2rN_p$ and $A \approx \pi r^2 N_T$ where N_p and N_T are respectively the number of C-type molecules in the periphery and in the entire domain. The maximum ($Q = 1$) corresponds to a perfectly circular domain shape. Therefore Fig. 2C plots Q for domains composed of polymers of different hydrophilic-hydrophobic proportions. After an initial equilibration time (~0.3 μs) and perhaps consistent with slightly lower P_2 order, the larger hydrophilic fraction C-domains appear more liquid-like (or soft gel-like) in showing stable quasi-circular shapes (see snapshot in Fig. 2 C) and a circularity Q that reaches a stable maximum. C-domains with a smaller hydrophilic fraction are more crystalline with Q fluctuating around different metastable states that represent more elongated, less circular shapes.

Although the results above are for the same number of C and N type molecules in each system, it should be added that the domain shape can be affected by the number of molecules in it. C-type molecules on the periphery are not so strongly confined

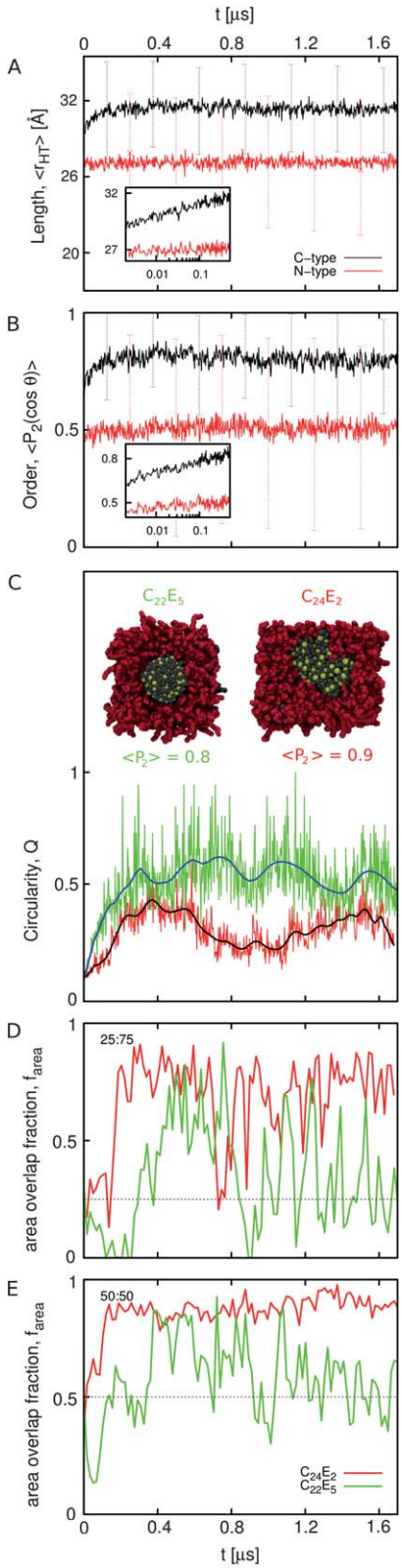

Fig. 2 Time series for various molecular and domain properties. **A, B**: Averaged polymer head-tail distance (A) and second Legendre polynomial (B). C-type (black) and N-type (red) polymers are shown for $C_{22}E_5$. The error bars represent mean deviations. The insets show the first 0.5 μs in log scale. **C**: The isoperimetric quotient for different polymer hydrophilic/hydrophobic proportion. Less ordered domains present more circular ($Q = 1$) and stable shapes. Characteristic snapshots showing domains of polymers with short ($C_{24}E_2$) and large ($C_{22}E_5$) hydrophilic fractions. **D, E**: Overlapped area fraction between C-domains in both leaflets. Membranes composed by a mixture C-type : L-type: 25 : 75 (D) and 50 : 50 (E). The low (red) and high (green) hydrophilic fraction are represented. Dotted black lines show the overlap value for stochastic mixtures. Most trajectories show a transition to large overlap states (registration) which seem stable. Larger overlapping values as well as small fluctuations are related to smaller hydrophilic fractions and larger—more crystalline—domains.

since they are in contact with the liquid phase (N-type molecules) and these provide more configurational freedom (suppressing < P_2 >). Therefore, when the domain size becomes larger, the relative number of molecules in the periphery is smaller, and the order in the domain affects shape most directly. Finite-size scaling is of course well known in all types of phase transition phenomena.

3.2 Registration

Concomitant with domain formation, interleaflet coupling leads to registration of some of the transient domains (see Fig. 1), but kinetics are complex. The final state certainly shows a single domain per leaflet that is closely matched in composition and shape by a domain in the opposite membrane leaflet, and the recurrence of the registered final state suggests stability.

To quantify interleaflet coupling we measured the C-domain area fraction (f_{area}) that overlapped with an equivalent domain in the opposed leaflet (see Fig. 2D and E). In all runs studied, the total number of molecules (C-type + N-type) was kept constant, and similar trends are seen: after a noticeable delay of up to ~0.3 μs the system suddenly locks into a new state with a larger value for f_{area} than the one corresponding to a stochastic mixture (~0.25 for 25 : 75 mixtures and ~0.5 for 50 : 50 mixtures). This suggests that the registered state is the more stable state even though thermal fluctuations can be large.

Raft registration is clearly affected by intrinsic (hydrophilic fraction) and extensive (domain size) surfactant properties that determine gel *vs.* crystalline phases. As mentioned, surfactants with smaller hydrophilic fractions yield more crystalline rafts ($C_{24}E_2$, red line) that exhibit (*i*) greater overlap and (*ii*) a more stable registered state with smaller fluctuations than gel-like rafts ($C_{22}E_5$, green line). Domain sizes also affect the coupling strength: larger rafts of the same surfactant yield more overlap and smaller fluctuations. Beyond the expectation that coupling is proportional to registered area larger domains also appear more ordered, which results in a sharper interface between ordered and disordered phases. It has been shown before that the interfacial tension of a polymer brush and a homopolymer melt can be written in terms of the square of the ordered phase concentration gradient.[48,49] More ordered domains will thus show a larger interfacial tension. Therefore as a general rule, the more ordered the domain, the stronger the interleaflet coupling.

A relationship between domain size and the strength of registration has been recently reported in ref. 50. The addition of EDTA to the spotted polymersomes extracts calcium from the outer leaflet and induces selective mixing of the domains. The dynamics of this process can be affected by the size of the

domains: the larger the domains the slower the dissolution. Our simulations also show a relationship between coupling strength and size of domains, and the molecular level of detail here reveals the important role of order of the domain.

3.3 Free energy analysis

Recurrence of the registration process reveals an intrinsic stability of this state. To probe this we determined the PMF for domains as a function of interleaflet overlap. The initial condition was a completely registered state ($f_{area} > 0.95$) of a 25 : 75 mixture. To minimize finite size limitations we use a membrane with an area 4 times larger than those in the previous simulations. The centers of mass of each domain were forced to move in an anti-parallel manner by applying forces in the plane of the membrane. The work calculated is then used to estimate the PMF[46] through the Jarzinsky equation.[51] Given that the heads of the polymers composing domains are practically frozen, the internal dynamics of the domains is minimal and domain shapes are not changing during pulling. Rotation of the domains was also negligible. These two conditions permit a one to one mapping between the separation of the center of masses and f_{area}. The PMF is thus plotted *versus* f_{area} in Fig. 3. The positive difference between the PMF in the final ($f_{area} = 0$) and initial states ($f_{area} = 1$) confirms the stability of the registered state. The strength of registration can be expressed as a free energy difference between the initial and final states, and is on the order of hundreds of kT. Thermal fluctuations are unlikely to overcome such barriers especially since the strength of interaction scales with the size of the domains. Compare for example the f_{area} values and fluctuations for $C_{22}E_5$ in Fig. 2D and E (green lines) and Fig. 4A (red line). Both domains are composed of the same surfactant and the mixture has the same composition (25 : 75) but the domain size is 4 times larger, thus generating a much larger overlap which suppresses fluctuations.

The molecular basis for registration is collective and physical with an interfacial tension between distinct "nano" phases: C-type and N-type surfactants possess identical hydrophobic chains but distinct headgroup interactions that ultimately generate two well defined phases. The segregation of ordered (C-domain) and disordered (N-type liquid) domains generates a contact surface in the midplane of the bilayer with an associated interfacial energy that drives registration.[7] The free energy penalty associated with registration is:

$$dF \propto \gamma \times dA$$

where F is the free energy, γ the mismatch free energy per unit area and A the mismatch area between upper and lower domains. The relationship of A to f_{area} is:

$$A \propto (1 - f_{area}).$$

If interfacial energy prevails as the driving force, a linear relationship between the PMF and f_{area} is expected. Conversely, Fig. 3 shows that PMF *vs.* f_{area} is a monotonically increasing but non-linear function with higher order terms. The linear relationship between mismatch area and free energy has been used to estimate the surface tension between lipid order and disordered phases[40] at least around the equilibrium position. Nevertheless, recent theoretical calculations suggest that this value is overestimated due to mismatch fluctuations comparable to the compositional correlation length.[39] In the very initial stages of our pulling ($f_{area} < 0.9$), the PMF is closer to past results but the

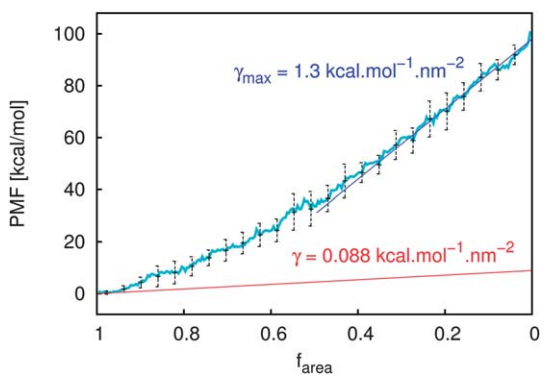

Fig. 3 Potential of mean force for domain pulling along the reaction coordinate ($f_{area} = 1$ complete overlap). In red, the expectation for free energy change due exclusively to interfacial tension term corresponding to that from ref. 40. The average domain area is ~100 nm^2. The non-linearity observed in the PMF indicates additional contributions beyond the interfacial tension term.

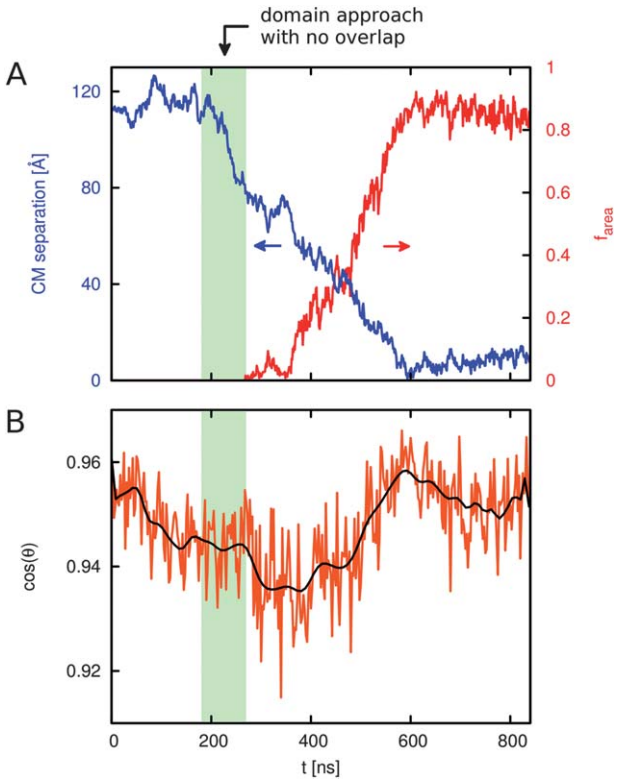

Fig. 4 Time evolution of describing registration. **A**: f_{area} (red line, right y-axis) and domain centers of mass separation (blue, left y-axis). **B**: domain principal axis of inertia with respect to the bilayer normal (z-axis). A tilt is observed during the period between 100–500 ns. The green shaded region indicates the window in which both domains move toward each other without being in contact.

slope is about ten-fold greater when the overlap vanishes. This suggests that the overall process is more than just minimization of the interfacial energy term. In other words we can say that the phenomenological γ is not simply the interfacial (constant) tension between order and disorder phases.

3.4 Structural and dynamical analysis of registration

The final state obtained after pulling apart shows completely "unregistered" domains ($f_{area} = 0$), which will be the starting point in the upcoming analysis. Separated C-domains are out of equilibrium and will move toward registration if permitted. We follow the evolution of a non-registered system after constraint release and analyze the structural changes in the bilayer. The evolution of the overlap area fraction is represented in Fig. 4 (red line): during the first 50 ns the isolated domains were kept apart by applying restraints. Once released, it takes ~250 ns for the domains to contact and then another 300 ns to completely register.

After the domains enter into contact f_{area} increases monotonically up to full overlap, which indicates a barrier-free movement of the domains towards each other. Fig. 4 also shows the time series for the center of mass separation of the domains (blue line). As expected, in the 300–600 ns window the domains displace one toward the other at a nearly constant speed. It is most remarkable that this movement starts 100 ns before the domains overlap (see green box in Fig. 4). This would suggest that the movement of one domain towards the other starts even before contact, *i.e.* the domains "feel" each other before starting to overlap. Transmembrane proteins have been shown to likewise interact through long-range distortions of the intervening lipid bilayer.[52,53]

The time series in the bottom part of Fig. 4 reveals the change in orientation of the largest domain's principal axis of inertia with respect to the bilayer normal during the registration. The value of the orientation angle θ increases ($cos\ \theta$ decreases), soon after the constraint is removed and up to 300 ns just when the domains make contact. After 400 ns the domain overlap is close to 0.5, and θ starts decreasing to values close to the original which is reached at 600 ns when the domains are completely registered.

To better understand the molecular basis of this driven movement of one domain towards the other we need to better describe the structure of the bilayer in both states, non-registered and registered. Fig. 5 shows the density profiles along the z-axis (perpendicular to the bilayer) for the polymer's hydrophilic terminal bead: top and bottom show densities for non-registered and registered systems respectively. Once domain registration occurs, protrusion of the gel-like phase (gray) into the water is clear.

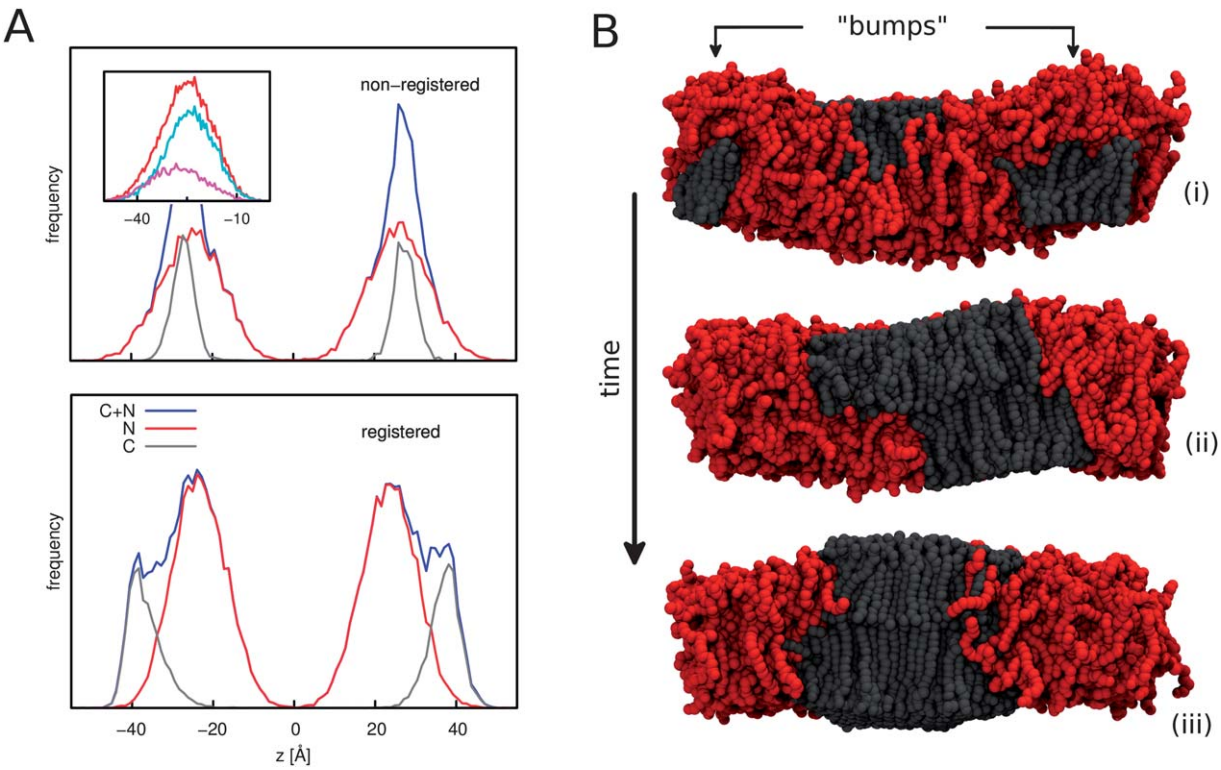

Fig. 5 **A**: Density profiles for the terminal hydrophilic bead of C (grey), L (red) and C + L (blue) type polymers along the perpendicular axis to the bilayer (z-axis), before (top) and after (bottom) registration. Non registered domains show no mismatch between L and C-type polymer headgroups but it is observed once registration force domains to protrude into the water. The inset shows the contributions to the L-type peak (red) before registration, the polymers sitting under the C-type domains (magenta) present a distribution that is shifted outwards compared to those under L-type (cyan). **B** Snapshots show the drifting of isolated C-domains into a registered final state. Only the polymers are shown. *i*: non-registered state reveals "bumps" induced by C-domains in the apposing liquid phases. *ii*: intermediate state showing partial registration and domain tilting with respect to the interface normal. *iii*: final registered state with domains protruding into the aqueous phase.

Protrusion of the C-domain into water is related to the fact that confinement, as mentioned above, forces the C-type molecules to stretch. Consequently, once the domains are registered the total height of the registered raft exceeds that of the surrounding liquid phase of N-type molecules. The energetic cost of this protrusion process, associated with line tension,[30,54] is caused by enlargement of the polymer-water interface and the hydrophobic mismatch between the N-type molecules and the domain, but it is also mitigated by domain bending. Such bending is noticeable in the long inward tails of the C-type headgroup distributions (Fig. 5A) as well as in snapshots (Fig. 5B). The inset plot shows two contributions to the liquid phase peak observed before registration. The N-type molecules that are right under a C-domain (magenta) are slightly wider and more exposed to the water than when under the N-type liquid phase (cyan). That is, the molecules sitting under a C-domain are pushed into the water. The difference between both distribution averages is ~8 Å. A plausible explanation is the stretch of the C-type molecules within the domains: in the initial configuration the headgroups for both types of molecules form a flat interface with water, *i.e.* C-domains are not protruding into the water (see Fig. 5B). The "excess length" or mismatch induces protrusions in the apposing liquid phase generating a "bump" in the otherwise flat structure. This protuberance is what leads to the shifting and widening of the density profile (red) to more negative values. As the C-domains move closer, the "bumps" on the apposing leaflet also get closer. This proximity induces a change in domain orientation with respect to the bilayer normal, and this tilting facilitates the encounter and slipping of one domain on top of the other. The final state shows a high degree of registration in which

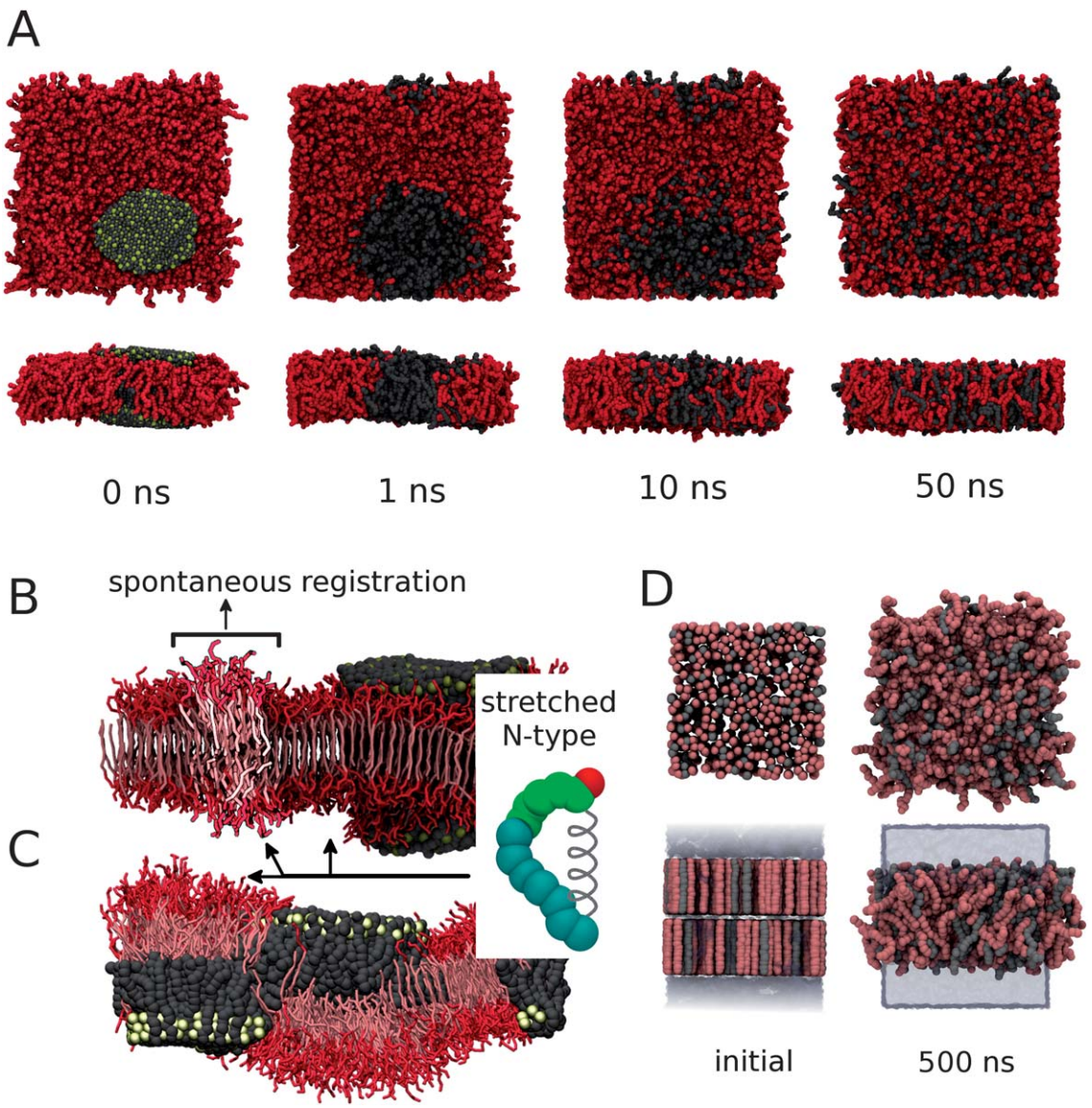

Fig. 6 Perturbations to ordering and registration. **A**: A few nanoseconds after calcium removal, lateral order is lost as shown in snapshots of the top and lateral view of the bilayer. **B, C**: An imposed spring force on each N-type polymer stretches the chain. The snapshot shows registered and non-registered C-type domain surrounded by stretched N-type molecules. **D**: Mixtures of two kinds of stretched N-type surfactants, pink and grey molecules extended to 28 Å and 32 Å, respectively.

the C-domains protrude into the water and also bend to reduce the height mismatch.

3.5 Crossbridging induces stretching and alignment while domains induce registration

Crossbridging by L-type particles is vital for registration. For the present system, lateral segregation is only possible with these crosslinkers. Snapshots in Fig. 6A show the time evolution of a segregated and registered system after the L-type particles are removed (analogous to the addition of EDTA to remove calcium). In about 50 ns the system is completely unregistered and the segregation is completely lost.

Initial simulations were also done with spring-based stretching of all N-type chains in a mixture to elongate all chains (C- and N-type) to a nearly equal extent (~32 Å). The stretched N-type chains are close to a crystalline state, but appear to wobble more than the calcium-crossbridged C-type chains. We simulated two initial states with the C-type domains being registered or not (Fig. 6B and C, respectively). In the first case, the presence of stretched N-type surfactants did not affect the stability and registration of the C-type domains. In the out of registry second case, the stretched N-type chains that are most aligned appear in the leaflet directly opposite to the C-type domains; the overall aspect of the membrane is also flatter than the analogous structure shown in Fig. 5B (top). Surprisingly there was also no initial evidence that such separated domains tended to interact on time scales seen in the interactions of Fig. 1–5. This seems consistent with the idea that local curvature in the domain vicinity helps raft registration. The energy source to achieve the required stretching of C-type surfactants is of course the condensation of L-type particles.

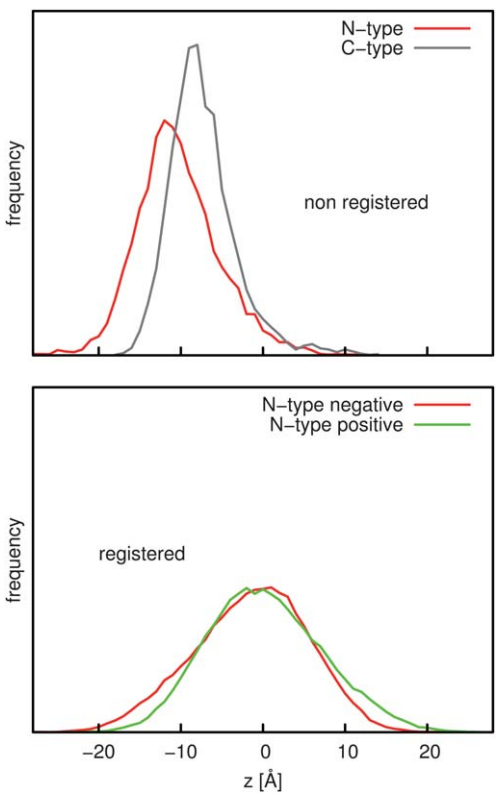

Fig. 7 Density profiles for the terminal hydrophobic beads. Top: non-registered systems, N-type surfactants from the negative leaflet ($z < 0$) are represented in red and C-type from the positive leaflet ($z > 0$) in grey. Bottom: registered system showing N-type from the positive (green) and negative (red) leaflet. Not only can a different level or interdigitation be observed but also a displacement of the midplane by ~10 Å.

Importantly, in the registered case of Fig. 6B we observed small domains of less aligned, protruding N-type chains which also seemed to induce a registered raft of less aligned molecules in the opposite leaflet. The domains also include some wobbling, stretched chains and so have an overall lower order than calcium-requiring C-type domains. Given the small size of such registered rafts of N-chains in a larger 'sea' of stretched N-chains, it is clear that crossbridging exerts additional effects on C-type chains, namely alignment of the chains.

Finally we checked that differences in the level of stretching are not sufficient to induce either lateral segregation or registration. We simulate a mixture of two differently stretched N-type surfactants: 28 Å and 32 Å which mimic the head-tail distances. Fig. 6D snapshots show that after 500 ns the system continues to be a mixture of both surfactants with no order of any kind observed.

4. Conclusions

Equilibrated mixtures here of C and N-type amphiphiles in the presence of cross-linker particles (L-type particles) show that C-domains in both leaflets are, in most cases, locked in a registered state. The strength of the coupling is related to the nature of the amphiphile as well as the size of the aggregates. Both factors favor raft registration if they induce more ordered (stretched and oriented) domains as they generally do (see Fig. 2A and B). A similar effect can be seen in "autophobic" dewetting of a polymer brush in contact with a homopolymer melt.[49,55,56] An interfacial tension arises between a disordered homopolymer and an end-adsorbed ordered layer with a critical role for the concentration profile of the brush: the sharper the profile (more stretched chains) the larger the interfacial tension.[49] In the present case of ordered rafts in bilayers the expected dewetting in the vicinity of both domains is minimized if the ordered "brushes" register. Analogous reasoning has been previously employed to account for the interleaflet coupling and colocalization observed in systems showing coexistence of both liquid ordered and disordered phases. Most past studies of lipid rafts and registration[5,57,58] have been focused in both theory and simulation,[40,59] on registration due to interfacial tension with an estimated value that fits only small perturbations here.[40] The lack of linearity seen in Fig. 3 suggests additional driving forces for the overall process.

Among other proposed mechanisms,[6,8,9,12,14–16] dynamic chain interdigitation likely provides some contribution to the registration process in lipid membranes.[8] However, rafts of the type simulated here register in polymer vesicles[31] even though synthetic polymer chains are always polydisperse and large enough to be highly flexible—thus opposing registration. Raft registration of charged lipid systems with calcium has also been seen,[32,38] despite shorter and more monodisperse lipid chains. The chains here are flexible but monodisperse and shorter than

the noted polymers, which seems a reasonable approximation of the various experimental systems. Nonetheless, a large chain entropy reduces the overall free energy, and our results in Fig. 5B suggest that N-type molecules have a larger degree of interpenetration with opposite leaflet N-type molecules than C-type (Fig. 5B). Fig. 7 shows that N-type hydrophobic terminal beads exhibit a different level of penetration in the opposite leaflet if the latter is composed of C-type or N-type surfactants. It can also be seen that the midplane is displaced ~10 Å. We have shown recently that overall interdigitation is very similar in registered and non-registered systems.[43] The apparent contradiction confirms that domain size and order are correlated. In our previous work domains were smaller and therefore less ordered which allowed the N-type molecules to have a similar level of penetration with both C-type and N-type surfactants. In the present work, larger and more ordered domains preclude good interdigitation with N-type surfactants.

One effect of both the midplane displacement and the poorer interdigitation of N-type and C-type is the observed "bump" near the domain. The conformational free energy contribution (Szleifer *et al.*[60]) can be estimated to be ~0.1 kT which is not large enough to account for the free energy difference observed in Fig. 3. Contributions from membrane curvature should therefore be considered, especially given the intense study of relationships between curvature and local composition in membranes.[14,61,62] Significant changes in the curvature of the bilayer do occur in the vicinity of C-type domains during registration (Fig. 5B). Similar to the curvature change observed for polymer-tethered phospholipid bilayers[58] where the pinning of certain lipids in one leaflet induces changes the curvature of the entire membrane, the unregistered C-domains cause deviations of the bilayer from a planar geometry, engendering protrusions in the opposite leaflet. We indeed see two distinct states: the seemingly wavy non-registered bilayer with "bumps" in liquid phase density (Fig. 5A top, Fig. 5B (*i*) and Fig. 7 top) and the flatter structure corresponding to the registered system (Fig. 5A bottom, Fig. 5B (*iii*) and Fig. 7 bottom). However, given the dimensions of the system we cannot predict how a larger membrane behaves.

Other sources of stabilization should be considered such as the minimization of line tension between regions of height mismatch. As highlighted in Fig. 4, the movement of one domain towards the other does not seem to be random before overlap. Lastly, the absence of charges in the model does not seem to limit insights into interleaflet coupling. While techniques employed here have a long record of success in coarse-graining real atomistic systems, here we show that registration of head-induced rafts is ultimately associated with collective phenomena based on differential order.

5. Acknowledgements

We would like to thank Prof. Andrea Liu and Dr Sharon Loverde for useful discussions.

References

1 D. Lingwood and K. Simons, *Science*, 2010, **327**, 46–50.
2 K. Jacobson, O. G. Mouritsen and R. G. W. Anderson, *Nat. Cell Biol.*, 2007, **9**, 7–14.
3 L. J. Pike, *J. Lipid Res.*, 2006, **47**, 1597–8.
4 M. Ikeda, A. Kihara and Y. Igarashi, *Biol. Pharm. Bull.*, 2006, **29**, 1542–1546.
5 V. Kiessling, J. M. Crane and L. K. Tamm, *Biophys. J.*, 2006, **91**, 3313–26.
6 D. Lingwood, J. Ries, P. Schwille and K. Simons, *Proc. Natl. Acad. Sci. U. S. A.*, 2008, **105**, 10005–10.
7 M. D. Collins and S. L. Keller, *Proc. Natl. Acad. Sci. U. S. A.*, 2008, **105**, 124–8.
8 S. May, *Soft Matter*, 2009, **5**, 3148–3156.
9 W. Lin, C. Blanchette, T. Ratto and M. Longo, *Biophys. J.*, 2006, **90**, 228–237.
10 R. D. Kornberg and H. M. McConnell, *Biochemistry*, 1971, **10**, 1111–20.
11 Y. Lange, J. Dolde and T. L. Steck, *Journal of Biological Chemistry*, 1981, **256**, 5321.
12 J. A. Hamilton, *Curr. Opin. Lipidol.*, 2003, **14**, 263.
13 K. Simons and D. Toomre, *Nat. Rev. Mol. Cell Biol.*, 2000, **1**, 31–39.
14 S. Leibler and D. Andelman, *J. Phys.*, 1987, **48**, 2013–2018.
15 T. McIntosh, S. Simon, D. Needham and C. Huang, *Biochemistry*, 1992, **31**, 2020–2024.
16 V. Schram and T. Thompson, *Biophys. J.*, 1995, **69**, 2517–2520.
17 K. Simons and E. Ikonen, *Nature*, 1997, **387**, 569–72.
18 A. Mukai, T. Kurisaki, S. B. Sato, T. Kobayashi, G. Kondoh and N. Hashimoto, *Exp. Cell Res.*, 2009, **315**, 3052–63.
19 Y. Zhang, K. A. Becker and E. Gulbins, *Chemistry and Physics of Lipids*, 2009, **160**, S2–S3.
20 M. Y. Lee, J. M. Ryu, S. H. Lee, J. H. Park and H. J. Han, *J. Lipid Res.*, 2010, **51**, 2082–9.
21 L. M. Pierini, R. J. Eddy, M. Fuortes, S. Seveau, C. Casulo and F. R. Maxfield, *J. Biol. Chem.*, 2003, **278**, 10831–41.
22 L. Bagatolli and E. Gratton, *Biophys. J.*, 2000, **78**, 290–305.
23 L. Bagatolli, *Chem. Phys. Lipids*, 2003, **122**, 137–145.
24 J. Crane and L. Tamm, *Biophys. J.*, 2004, **86**, 2965–2979.
25 C. Dietrich, L. Bagatolli, Z. Volovyk, N. Thompson, M. Levi, K. Jacobson and E. Gratton, *Biophys. J.*, 2001, **80**, 1417–1428.
26 B. Stottrup, S. Veatch and S. Keller, *Biophys. J.*, 2004, **86**, 2942–2950.
27 S. Veatch, I. Polozov, K. Gawrisch and S. Keller, *Biophys. J.*, 2004, **86**, 2910–2922.
28 S. L. Veatch and S. L. Keller, *Biophys. J.*, 2003, **85**, 3074–3083.
29 S. Veatch and S. Keller, *Biochim. Biophys. Acta, Mol. Cell Res.*, 2005, **1746**, 172–185.
30 T. Baumgart, A. T. Hammond, P. Sengupta, S. T. Hess, D. A. Holowka, B. A. Baird and W. W. Webb, *Proc. Natl. Acad. Sci. U. S. A.*, 2007, **104**, 3165.
31 D. Christian, A. Tian, W. Ellenbroek, I. Levental, K. Rajagopal, P. Janmey, A. Liu, T. Baumgart and D. Discher, *Nat. Mater.*, 2009, **8**, 843–849.
32 I. Levental, D. Christian, Y. Wang, J. Madara, D. Discher and P. Janmey, *Biochemistry*, 2009, **48**, 8241–8248.
33 L. Carvalho, C. Ramos and C. RoyPicart, *Biophys. J.*, 2008, **95**, 4348–60.
34 D. Discher and A. Eisenberg, *Science*, 2002, **297**, 967.
35 D. J. Pochan, Z. Chen, H. Cui, K. Hales, K. Qi and K. L. Wooley, *Science*, 2004, **306**, 94–7.
36 Y. Won, H. Davis and F. Bates, *Science*, 1999, **283**, 960.
37 L. Zhang, K. Yu and A. Eisenberg, *Science*, 1996, **272**, 1777.
38 Y. Geng, F. Ahmed, N. Bhasin and D. E. Discher, *J. Phys. Chem. B*, 2005, **109**, 3772–9.
39 G. G. Putzel, M. J. Uline, I. Szleifer and M. Schick, *Biophys. J.*, 2011, **100**, 996–1004.
40 H. Risselada and S. Marrink, *Proc. Natl. Acad. Sci. U. S. A.*, 2008, **105**, 17367.
41 M. Laradji and P. Kumar, *J. Chem. Phys.*, 2005, **123**, 224902.
42 W. Shinoda, R. DeVane and M. L. Klein, *Mol. Simul.*, 2007, **33**, 27–36.
43 D. A. Pantano, M. L. Klein, D. E. Discher and P. B. Moore, *J. Phys. Chem. B*, 2011, **115**, 4689–95.
44 S. Plimpton, *J. Comput. Phys.*, 1995, **117**, 1–19.
45 W. Humphrey, A. Dalke and K. Schulten, *J. Mol. Graphics*, 1996, **14**, 33–38.
46 S. Park and K. Schulten, *J. Chem. Phys.*, 2004, **120**, 5946–61.
47 S. Izrailev, S. Stepaniants, B. Isralewitz, D. Kosztin, H. Lu, F. Molnar, W. Wriggers and K. Schulten, *Computational Molecular Dynamics: Challenges, Methods, Ideas*, 1998, **4**, 39–65.

48 D. Broseta, G. H. Fredrickson, E. Helfand and L. Leibler, *Macromolecules*, 1990, **23**, 132–139.
49 K. Shull, *Faraday Discuss.*, 1994, **98**, 203–217.
50 A. Tian, PhD thesis, University of Pennsylvania, 2010.
51 C. Jarzynski, *Phys. Rev. Lett.*, 1997, **78**, 2690–2693.
52 N. Dan, P. Pincus and S. a. Safran, *Langmuir*, 1993, **9**, 2768–2771.
53 K. S. Kim, J. Neu and G. Oster, *Biophys. J.*, 1998, **75**, 2274–91.
54 S. Loverde, F. Solis and M. Olvera de la Cruz, *Phys. Rev. Lett.*, 2007, **98**, 8–11.
55 G. Reiter and R. Khanna, *Phys. Rev. Lett.*, 2000, **85**, 5599–5602.
56 G. Reiter and R. Khanna, *Phys. Rev. Lett.*, 2000, **85**, 2753–2756.
57 S. Garg, J. Rühe, K. Lüdtke, R. Jordan and C. a. Naumann, *Biophys. J.*, 2007, **92**, 1263–70.
58 M. A. Deverall, S. Garg, K. Ludtke, R. Jordan, J. Rühe and C. Naumann, *Soft Matter*, 2008, **4**, 1899–1908.
59 M. D. Collins, *Biophys. J.*, 2008, **94**, L32–4.
60 I. Szleifer, A. Ben-Shaul and W. Gelbart, *J. Phys. Chem.*, 1990, **94**, 5081–5089.
61 R. Parthasarathy, C.-h. Yu and J. T. Groves, *Langmuir*, 2006, **22**, 5095–9.
62 A. Roux, D. Cuvelier, P. Nassoy, J. Prost, P. Bassereau and B. Goud, *EMBO J.*, 2005, **24**, 1537–1545.